A Wavelength Tunable Multi-Section PIC as an Upstream Transmitter for TWDM Networks

Ankit Sharma , *Graduate Student Member, IEEE,*
Aleksandra Maria Kaszubowska-Anandarajah , *Senior Member, IEEE,* Michael Wallace, Gaurav Jain,
Jules Braddell, Frank Smyth, and Prince M. Anandarajah , *Senior Member, IEEE*

Abstract—In this paper, we demonstrate a novel multi-section directly modulated laser transmitter for upstream operation in the application of time wavelength division multiplexing (TWDM) architecture. The photonic integrated circuit (PIC) is fabricated using a regrowth-free process that favors simplified and fast manufacturing. The PIC is based on a master-slave configuration, with an addition of a variable optical attenuator (VOA) section between them, and a semiconductor optical amplifier (SOA) at the output. The VOA enables control of the optical injection from the master to the directly modulated slave laser improving the transmission performance. The integrated SOA section at the output is used to boost or turn off the optical output power of the transmitter, thereby enabling burst mode operation. Experimental results show that the PIC can be tuned to four wavelength channels on a 100 GHz frequency grid. We also demonstrate that each channel achieves error-free performance (bit error ratio $< 10e^{-9}$), when modulated with 10 Gbps signal and transmitted over 25 km and 50 km fiber. The SOA-based output disable feature of the PIC delivers more than 60 dB attenuation.

Index Terms—And photonic integrated circuits (PICs), chromatic dispersion, high-speed transmitters, monolithic integrated circuits.

I. INTRODUCTION

PASSIVE optical networks (pons) have been evolving over the past couple of decades, to fulfill the demand for high data rates in access networks. There has been a substantial amount of progress since the first PON architecture was introduced [1], [2], [3]. APON and BPON were the first

of the PON generations that handled telephone, internet, and video services. Later, EPON, GPON, XG-PON, XGSPON, and NGPON-1 have sequentially been introduced with improved uplink and downlink speed, additional services, greater split ratio, while maintaining backward compatibility. In the development of PONs several multiplexing techniques, including time division multiplexing (TDM), wavelength division multiplexing (WDM), or hybrid time/wavelength division multiplexing were considered. TDM benefits from a simple architecture [4], but the channel is divided among all the users. In WDM PON, theoretically, a dedicated channel is assigned to each user, which provides a significant increase in the uplink rates. A wavelength filter could be used to separate the specific WDM signal to be sent to a user [5], thereby reducing the overall signal splitting loss of the system. However, the requirement of a wavelength specific filter complicates the receiver architecture, reduces the number of users that can be served, and increases the cost of deployment. Hence, other solutions that could serve a large number of users whilst delivering a high channel capacity such as OCDM-WDM [6] and OFDM-WDM [7] were researched. However, it is important for any such solution to be able to support backward compatibility/ coexistence on the same fiber infrastructure at low cost. One such technique entails the use of time wavelength division multiplexing (TWDM) architecture, which is standardized by ITU-T G989.2 as the next-generation passive optical network-2 (NGPON-2) [8].

NGPON-2 exhibits an aggregate capacity of 40 Gbps and 10 Gbps in downstream and upstream directions, respectively. As any access network technology, the NGPON-2 transceiver needs to meet the target specifications in an inexpensive manner. Hence, photonic integration is considered as a promising solution, providing cost effective, energy efficient, compact, and reliable devices. Photonic integrated directly modulated lasers (DML) are known to be a simpler and a more cost-efficient approach in comparison to externally modulated lasers (EMLs) [9]. Some DML-based integrated transmitters for short reach applications have been demonstrated in [10], [11], [12], [13]. However, the proposed schemes suffer from a few different challenges such as sophisticated fabrication, low yield, and a degraded quality of the transmitted optical signal due to chirp induced chromatic dispersion.

In this paper, we demonstrate a proof-of-concept device by expanding previous work carried out in [14] and showing the detailed characterization of a PIC transmitter demonstrating
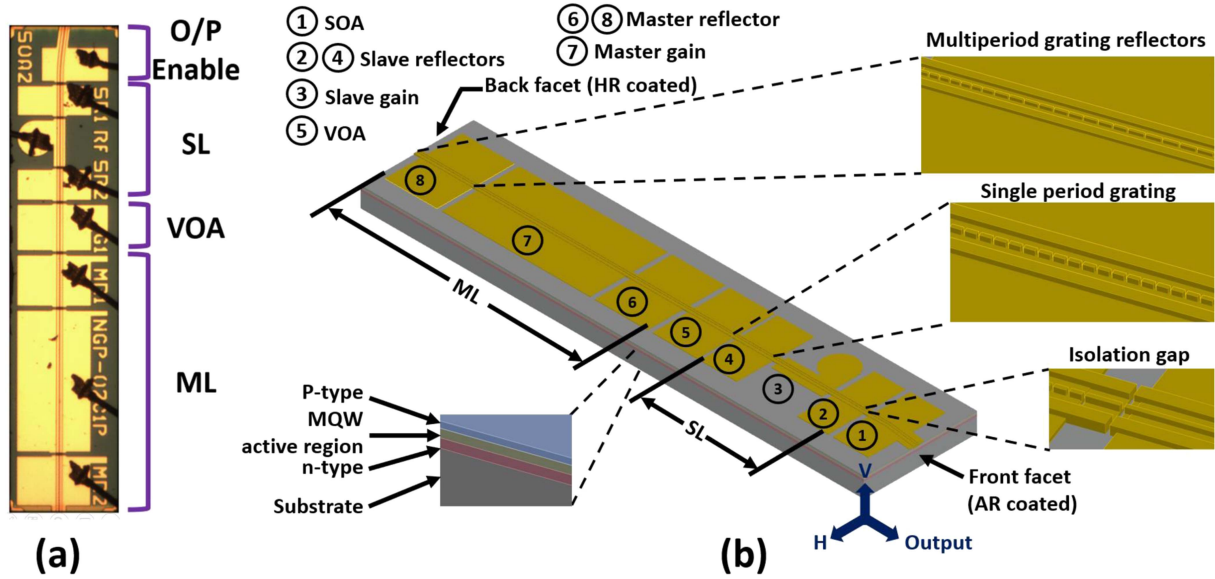
Fig. 1. (a) Layout of the chip and (b) 3-dimentional design and architecture of 8-section PIC. Inset: SL-slave laser, ML-master laser, VOA-variable optical attenuator, MQW-multiple quantum wells, SOA-semiconductor optical amplifier, AR-anti-reflective coating, HR-high-reflective coating, V-vertical and H-Horizontal.

wavelength tunability, low cross channel interference, long reach, and burst mode transmission. The proposed device consists of a VOA controlled master-slave laser arrangement analogous to [15] and an integrated semiconductor optical amplifier (SOA) at the output stage. The master-slave architecture allows the device to operate in an injection-locked regime. This brings a suite of benefits, such as an improved dynamic response and reduced frequency chirp, as previously showed in [16], [17], [18]. As an improvement over the previously demonstrated 4-section device [19], the chip presented here features precise and independent control of the injection. This control allows for the operating wavelength of the master and slave lasers to be tuned with a negligible change in output power. The integrated SOA at the output stage facilitates two important features, acting firstly as an optical amplifier, and secondly as an optical switch to generate a burst mode signal. This multi-section device can generate four injection locked (IL) wavelength channels with each one capable of being directly modulated with an on-off keyed (OOK) data signal at 10 Gbps. The performance of all four modulated wavelengths is measured when transmitted over 25 km and 50 km of standard single mode fiber (SSMF). In addition, we demonstrate that the PIC meets the NGPON-2 power-when-not-enable (PWNE) requirements and features low adjacent channels interference.

The remainder of paper is organized as follows: Section II explains the design of the PIC and includes a detailed description of the integrated sections. Section III consists of the static characterization of the slave laser and provides details on achieving injection locking. Section IV contains a discussion on an algorithm used to find four injection locked wavelengths on a 100 GHz grid. Section V presents the effect of optical injection on the transmission performance of the PIC at each of the four injection locked wavelengths. In Sections VI and VII the enable/disable and burst mode signaling features of the PIC are examined. Finally, Section VIII summarizes the paper.

II. DEVICE DESIGN AND FABRICATION

The PIC transmitter is manufactured using an identical epitaxial composition and the technology adopted for the fabrication of the ridge waveguide is also the same as that described in [20]. The chip is ∼2 mm long and it is divided into four main sections: master laser (ML), VOA, slave laser (SL), and an SOA (as shown in Fig. 1(a)). The front and back facets are anti-reflective (AR) and high reflective coated, respectively. The waveguide at front section is angled at 7° to minimize the optical feedback [21]. Fig. 1(b) represents the detailed 3-dimensional architecture of the 8-section PIC. The SL and ML are formed by introducing gain sections that are sandwiched between two reflector sections. The length of the ML and SL are 1126 μm and 485 μm respectively. The reflectors MR1, and MR2 are formed by making 24 slots of three distinct periods. Multi-period gratings have been reported to yield a higher SMSR in comparison with single period gratings [22]. Similarly, the slave gain (SG) between the SR1 and SR2 sections forms the SL. The slave reflectors have a single period order grating structure. It is important to note that the length of the SG section is designed to be much shorter than MG section to reduce the photon lifetime and achieve a high modulation bandwidth. For the same reason, the contact pad of the SG section is kept small (150 μm diameter) thereby reducing the RC time constant (lowering the effect of parasitic capacitance). A short (221 μm) gain section, introduced between the ML and SL, serves as a VOA. Finally, the last section close to the output facet, is a 230 μm long semiconductor optical amplifier (SOA) to enable absorption, amplification and optical gating. The SOA section is kept short to support fast turn on-off operation. To isolate the flow of current between adjacent sections, a slot in the p-region with a depth of 1.35 μm and width of 1.15 μm is introduced. In addition, a 10 μm gap is also maintained between the all the contact pads.
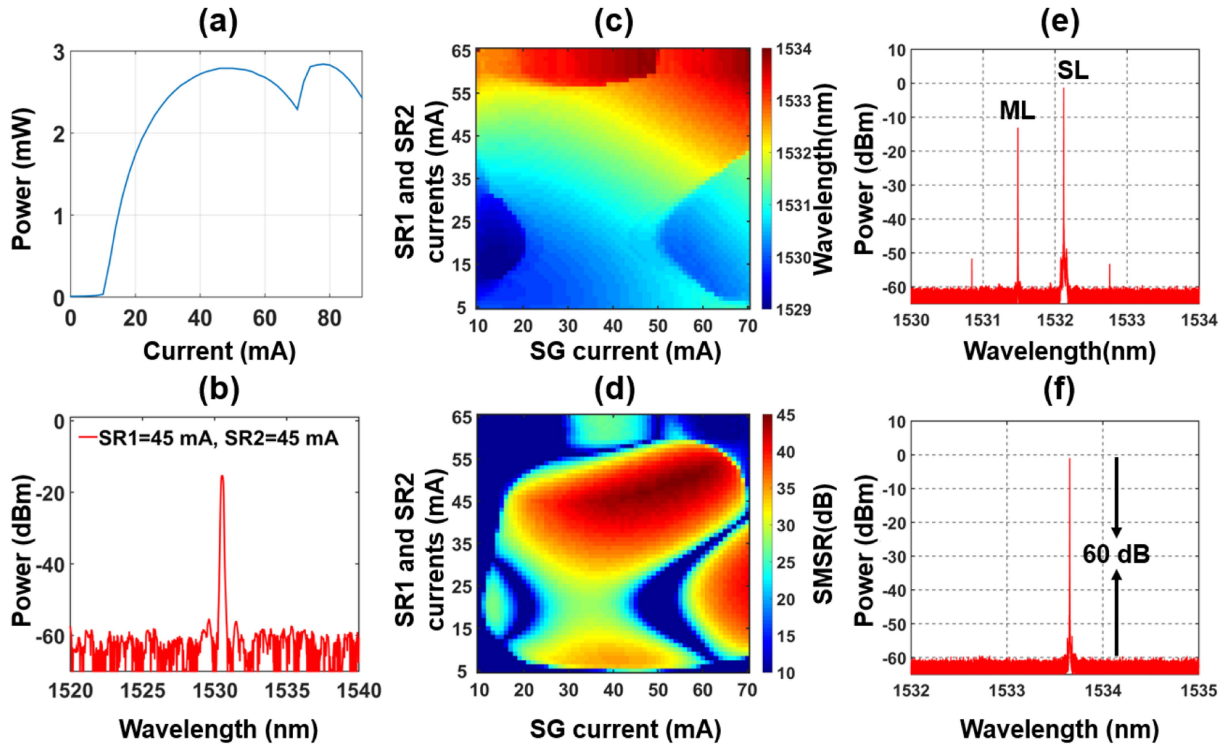
Fig. 2.   (a) L-I characteristic of slave laser, (b) Spectra of slave laser at SG = 40 mA, SR1 = 45 mA and, SR2 = 45 mA, (c) Wavelength map, (d) SMSR map, (e) ML and SL lasing independently, and (f) Spectrum of an injection locked operating point.

III. STATIC CHARACTERIZATION OF SLAVE LASER

To characterize the performance of the device, first a subcarrier printed circuit board (PCB) is manufactured containing a $50\,\Omega$ grounded coplanar waveguide-based transmission line and direct current (DC) contact pads. After that, the chip is mounted, and each section (except the SG section) is wire bonded with the gold pads of the subcarrier PCB. The contact pad of the SG section is wirebonded to a matching resistance ($34\,\Omega$) soldered on a $50\,\Omega$ radio frequency (RF) track [20]. The PCB is then mounted on a thermo-electric cooler (TEC). The output of the transmitter is coupled to a conical lens fiber mounted on a 3-axis auto-aligner, which plays a crucial role in maintaining optimum coupling of the light to a lensed fiber. Initially, only the SOA, SR1, SG and SR2 sections are biased to determine the standalone performance (L-I and spectrum) of the SL.

To measure the L-I curve, the bias currents of the SOA, SR1 and SR2 are set to 21 mA, 45 mA and 45 mA, respectively. SL exhibits a single mode operation when SR1 and SR2 are biased above 40 mA. Moreover, SR1 and SR2 act as an active DBR and require a minimum current of 21 mA. The slot-based reflectors introduce high loss due to scattering, which can be compensated by the gain of the active DBR section [23], [24]. The DC current of the SG section is swept, from 0 to 90 mA in steps of 1 mA, and the output power of the device is recorded using a wide area photodiode. The L-I characteristic plotted in Fig. 2(a) shows that the threshold of the SL is ~ 12 mA. A thorough investigation of the SL is carried out by extracting heat-maps of the peak wavelength and SMSR. To this effect,

the current in the SG section is swept from 10 mA to 70 mA (at steps of 1 mA), the biases of the SR1 and SR2 are swept from 5 mA to 65 mA (with an increment step of 1 mA, same current applied to both reflectors)) and the SOA section is biased at 21 mA. The measured peak wavelength and SMSR maps are showed in Fig. 2(c) and (d) respectively. The plots demonstrate a wavelength tunability of the SL from 1529.5 nm to 1533 nm at an SMSR > 30 dB. An optical spectrum (shown in Fig. 2(b)) is then captured for the following sections biases SR1 = 45 mA, SR2 = 45 mA, and SG = 40 mA. The main reason for choosing a 45 mA bias for SR1 and SR2 is that at these settings the SL portrays the lowest threshold current and an SMSR > 45 dB. Subsequently, we proceed to confirm the independent lasing of the ML and SL. To do this, we apply the following currents to the device: SR1 = 42 mA, SR2 = 45 mA, SG = 40 mA, MR1 = 20 mA, MR2 = 45 mA, MG = 40 mA, VOA = 4 mA. The optical spectrum in Fig. 2(e) shows ML and SL lasing at 1531 nm and 1532 nm respectively. To obtain the injection locking point, the currents of MR1, MG, and MR2 are gradually increased until a single mode optical spectrum with a high SMSR is achieved. As shown in Fig. 2(f), the injection locked wavelength portrays an SMSR of 60 dB.

IV. OPTIMIZATION OF INJECTION LOCKING

Fig. 2(f) proves the ability to achieve injection locking of the SL at a single wavelength. To verify the compatibility of the transmitter with the NGPON-2 wavelength grid, a more comprehensive test is performed. The procedure of finding an
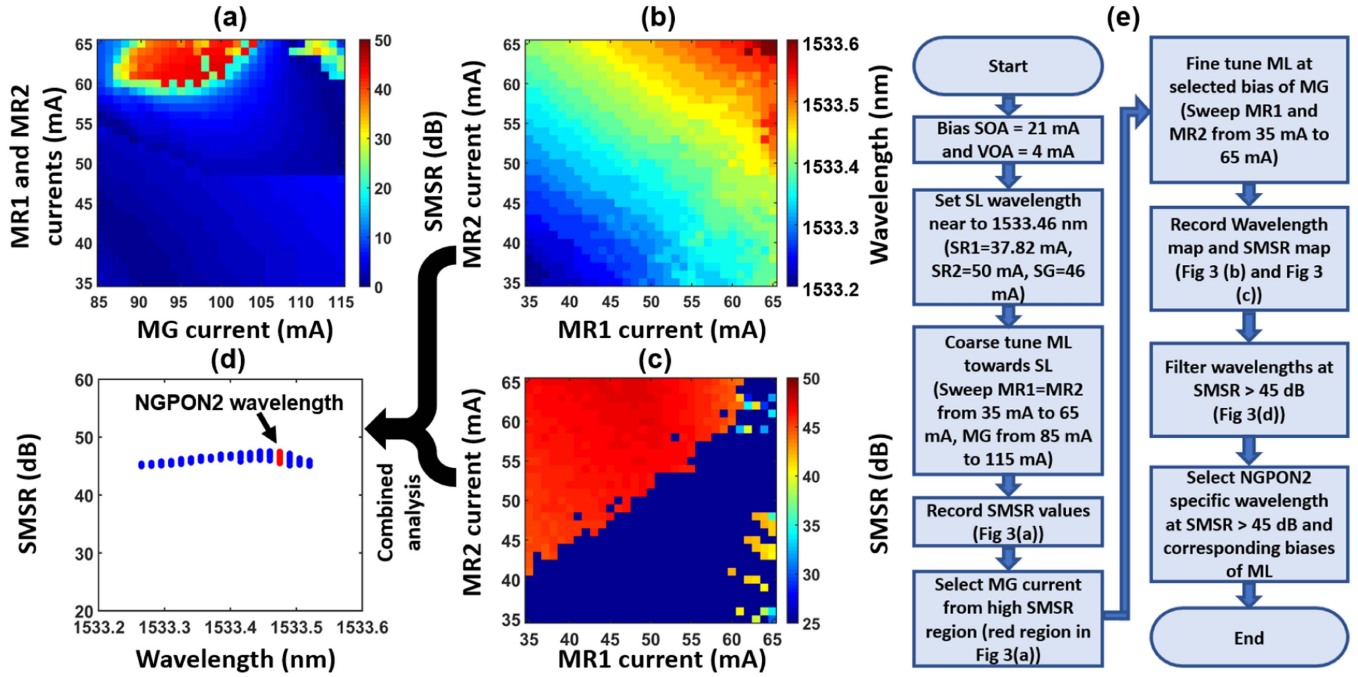
Fig. 3. (a) SMSR map of SL in course tuning of ML (b) Wavelength map, (c) SMSR map in fine tuning of ML at $MG = 100$ mA, (d) Extracted injection locked wavelengths (blue) and NGPON-2 specific wavelength (red), (e) Flow chart for finding injection locked wavelength.

injection locked wavelength is captured as a flowchart and shown in Fig. 3. It consists of two main steps: a coarse-tuning and fine-tuning operation of the ML. The ML can be tuned by varying effective refractive index by supplying current in each section as described in [25]. The steps applied to find an IL wavelength at 1533.46 nm are as follows; first, the SL is tuned to one of the NGPON-2 wavelengths and a coarse tuning operation is performed. To initiate this operation, the sections SR1, SG and SR2 are biased at 37.82 mA, 50 mA, and 46 mA, respectively, at which point the SL lases at 1533.25 nm (close to the target wavelength). The SOA section is driven at transparency (21 mA) and kept unchanged in further measurements. Subsequently, the ML sections MR1, MG, and MR2 are biased at 35 mA, 85 mA, and 35 mA. At this bias, the ML wavelength is slightly below the SL (1532.8 nm). Thereafter, the current in the MG section is swept from 85 mA to 115 mA in steps of 1 mA, while MR1 and MR2 currents are simultaneously varied from 35 mA to 60 mA in steps of 1 mA. This two-dimensional scan (MR1 & MR2 current vs MG current) tunes the ML wavelength towards that of the SL. As soon as ML enters the injection locking range, the ML pulls the SL to its wavelength. By measuring the SMSR during this current sweep and identifying the regions with an SMSR value exceeding 40 dB, it is possible to identify all IL wavelengths (the red region in Fig. 3(a)). Fig. 3(a) shows that the SL tends to be injection locked when the MG section is biased between 90 mA to 102 mA. In the second step (fine-tuning operation), the same investigation is carried out by biasing the MG at 100 mA and carrying out a two-dimensional current sweep of the MR1 and MR2 sections. Again, the wavelength and SMSR are plotted as heat-maps which are shown in Fig. 3(b) and (c) respectively. In Fig. 3(c), the region in red shows all the possible IL wavelengths.

To find the settings for the desired channel (1533.46 nm), all achievable wavelengths with SMSRs > 45 dB are extracted and plotted in Fig. 3(d). The red dots in Fig. 3(d) corresponds to the target IL wavelength, showing that there are several bias current combinations delivering the target channel. Amongst these, the operating point providing the highest SMSR is chosen for further characterization. Firstly, the optical linewidth of the IL signal is measured using the delayed self-heterodyne method [26]. The result is then compared with the optical linewidths of the free running ML and SL. It is well known that the linewidth of the IL SL follows the linewidth of the ML, thus this measurement can be used to further verify whether an effective IL is achieved [27], [28]. The measured linewidth of the SL, ML, and injection locked SL are ~38.5 MHz, ~6.7 MHz, and ~7.1 MHz with uncertainty of ±0.4 MHz, respectively. We attribute the slight difference in linewidth of IL SL and the ML to a measurement error. The same procedure is repeated for the remaining three NGPON-2 wavelengths (1532.68 nm, 1534.25 nm, 1535.02 nm). The overlaid spectrum of all four wavelengths on the 100 GHz grid, required for the upstream transmission, measured with the aid of a high resolution (0.16 pm) optical spectrum analyzer, are shown in Fig. 4. The output power of the PIC at IL1, IL2, IL3, and IL4, when SOA is biased at 21 mA, is 3.16 dBm, 2.71 dBm, 2.94 dBm, and 2.42 dBm, respectively. The power can be enhanced to 7.02 dBm, 7.46 dBm, 7.51 dBm, and 7.05 dBm by increasing the SOA current to 30 mA. The difference in peak power between the wavelength channels is due to the misalignment of the lens fiber (mounted on 3-axis translation stage) caused by minor thermal variations that are not compensated by the temperature control arrangement used.
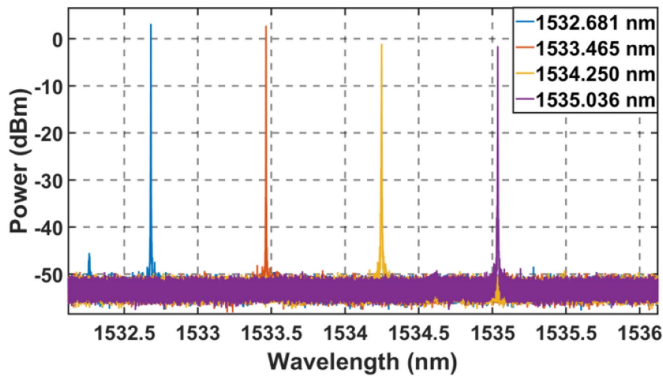
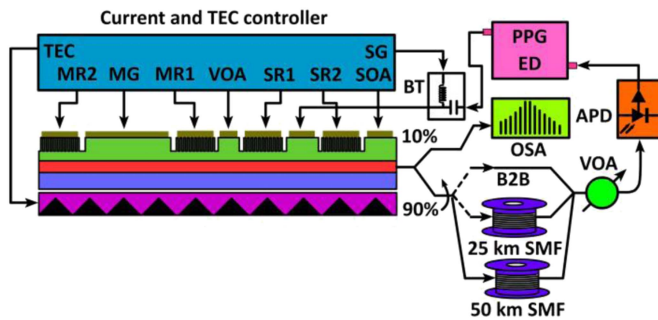Fig. 4.   Spectrum of four injection locked signals on a 100 GHz grid.

Fig. 5.   Experimental setup to perform transmission at each IL wavelength and measure corresponding BER.
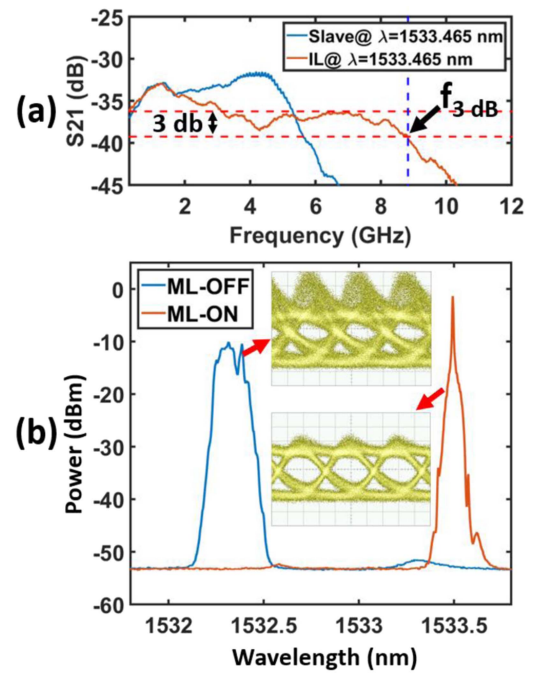

Fig. 6.   (a) Modulation response of SL (blue) and injection locked SL (orange). (b) a Comparison of optical spectrum of modulated SL: Without the injection (blue) and injection locked (orange). Inset: Eye diagrams of free running and optically injected SL.

V. DATA TRANSMISSION

Having determined the static performance of the device, we then move to investigate its dynamic operation. Firstly, the frequency response of the SL in a free running and optical injection scenario are characterized, to ensure the transmitter can support a data rate of 10 Gbps. As shown in Fig. 6(a) the 3 dB bandwidth of the free running SL is measured to be ~ 5.4 GHz, which is increased to ~ 8.82 GHz, due to the injection locking [27]. As this is sufficient for the 10 Gbps transmission rate, we proceed to test the system performance of the directly modulated transmitter at each of the four wavelengths shown in Fig. 4. The experimental setup used is shown in Fig. 5. First, all sections of the PIC are biased using the values identified in the previous section. A non-return to zero (NRZ) 10 Gbps pseudo random bit sequence (PRBS) of the order 2^{15}-1 and a peak-to-peak level of 2V, is generated by a pulse pattern generator (PPG). The generated signal is combined with a DC current using a wideband bias-tee and applied to the RF pad of SG section of the PIC. The modulated optical signal is then coupled into a 90:10 coupler, with the 10% output connected to the fiber auto-aligner and the 90% output used for the performance testing.

An optical spectrum of the modulated SL is captured at the transmitter and compared under two cases: without and with the injection (see Fig. 6(b)). In the first case, the spectrum (blue line) is broader because of the presence of frequency chirp induced by direct modulation. However, we clearly see a reduction in the spectral width in the second case (orange line)

[18]. The wavelength of the injection locked SL is red-shifted due the injected/induced change in the effective refractive index [29]. In addition, we see a clear eye pattern when the SL is injection locked in comparison to the free running SL. This can be attributed to the damped relaxation oscillations, and the reduced amplitude fluctuations [30]. Subsequently, the impact of the injection level on the spectral width of the SL is further investigated by varying the bias of the VOA section (higher bias corresponds to a higher optical injected power / lower optical attenuation).

The increase in VOA current reduces the optical attenuation and increases the power injected from the ML, leading to a reduction of the frequency chirp. Fig. 7 shows the spectra of the SL for three values of the VOA current. From the plot it can be seen that the spectral width (chirp) is reduced significantly as the level of injection is increased. In addition, the appearance of the "rabbit ears" in the spectrum, indicating the presence of transient chirp [31], is also reduced. The measured 20-dB spectral width at VOA bias currents of 1 mA, 2 mA, and 4 mA are ~ 98.7 pm, ~ 94 pm, and ~ 92 pm, respectively. While the lowest spectral width is obtained when the VOA bias is set at 4 mA, for the remainder of the test the VOA current is set at 2 mA, where there is a balance between the reduction of chirp and extinction ratio (ER). A high level of optical injection significantly reduces the chirp, but at the same time reduces the threshold of the laser, which results in a degraded ER. The ER for 1 mA, 2 mA, and 4 mA bias current applied to the VOA is $\sim$3.9 dB, $\sim$3.8 dB, and $\sim$3.6 dB, respectively. Hence, the VOA plays an important role in managing the trade-off between the chirp and ER. Another
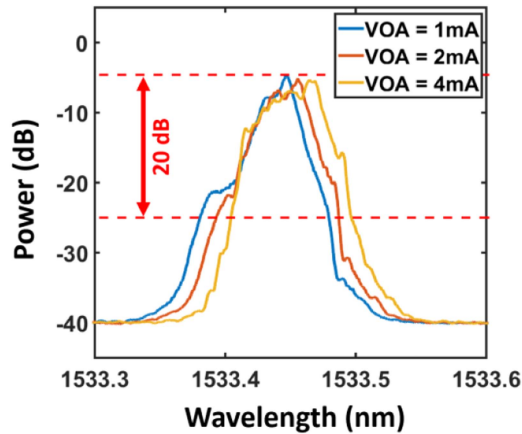
Fig. 7.   Effect of VOA bias on frequency chip.

important observation is the fact that the wavelength of the SL remains almost constant for all three VOA biases, indicating the ability to optimize the injection level without affecting the operating point of the SL. This is a significant improvement in comparison to the previous versions of the chip, which did not have the VOA section. To determine the ER for each of the wavelength channel, the output of the transmitter is fed to a DC-coupled photodiode. The measured ER values, for each of the injection locked operating points IL1, IL2, IL3, and IL4, and their corresponding average output power levels, are 3.6 dB, 3.8 dB, 4.1 dB, 4.8 dB and 6.0 dBm, 5.66 dBm, 5.81 dBm, 4.81 dBm, respectively. The measured ER for IL3 and IL4 is 0.1 dB and 0.8 dB higher than the specified limit of 4 dB. However, IL1 and IL2 require 0.4 dB and 0.2 dB improvement in ER, respectively. The ER can be improved by shortening the cavity length of SL to increase the modulation response, and reducing the mirror losses to enhance the slope efficiency by optimizing the slot width, slot depth, and period order of slot grating.

Next, we carry out bit error ratio (BER) measurements for all channels, by launching the signal into an avalanche photodiode (APD). The received optical power (ROP) level is controlled and measured using an external VOA with an inbuilt power meter. The output of the APD is then connected to an error detector (ED) and the performance of the individual channels (BER) is measured in a back-to-back (B2B) scenario and after 25 and 50 km fiber transmission. The resultant plots of the BER versus the ROP for all four channels are shown in Fig. 8. From the figure it can be seen that not all channels perform equally. For the 50 km transmission, IL1 and IL3 show the worst and the best performance respectively. We would attribute the relatively poor B2B performance of IL1 to the lower ER (3.6 dB). On the other hand, the largest transmission penalty is observed for IL4 ($\sim$2 dB at a BER of 1e^{-9}). This could be ascribed to the lower level of optical injection used leading to the highest degree of chirp thereby resulting in a larger dispersion penalty. Nevertheless, for all the IL points a BER better than 5e^{-8} is achieved, even after 50 km of uncompensated fiber transmission, which is a significant result for a directly modulated transmitter.

It stems from the reduction of the frequency chirp introduced by the external, which enables an extension of the transmission distance.

VI. POWER WHEN NOT ENABLE (PWNE)

An acceptable transmitter for NGPON-2 must comply with the limit of PWNE, which limits the maximum output optical power spectral density (PSD) when the burst is not being transmitted to -62.6 dBm [8]. To meet the PWNE in the fabricated transmitter, an SOA is integrated at the output of the device, to allow disabling the output of the transmitter when no data is being sent (blanking the output power without the need to turn off the laser). This is achieved by toggling the SOA section between transparency or amplification (bias current $\geq$ 18 mA) and absorption (bias current $=$ 0 mA). Fig. 9 shows the comparison of the measured output optical spectrum, when the SOA is biased at 21 mA (blue trace) and 0 mA (orange trace), resulting in the change in the peak output power of the transmitter from 0 dBm to -60.77 dBm. To meet the specified power level for PWNE, the VOA is turned also off to attenuate the optical power from the ML and the SOA is reverse biased to increase the absorption of the light. This way the output power of the PIC drops below -62.6 dBm, which meets the specified PWNE limit for the NGPON-2 transmitter. In a future design, an additional SOA section at the output can be integrated, which can provide high optical absorption when it is turned-off. In the updated design the desired PWNE can be obtained without turning off other sections of the PIC.

VII. OUT-OF-CHANNEL (OOC) POWER MEASUREMENT IN BURST-MODE TRANSMISSION

Another requirement of the NGPON-2 standard that we tested on the proposed transmitter is the out-of-channel power-spectral-density (OOC-PSD). This requirement aims to minimize the cross-channel interference within the network. The OOC-PSD sets the maximum level of the PSD that a transmitter can generate outside of the operational channel. To verify the compliance with the OOC-PSD, the spectrum of the transmitter in burst mode is measured and compared with the standard described in [8]. For this test, the SOA is turned on and off during the burst mode operation. We generate a 62.5 μs, 50% duty cycle, 2V pk-pk square wave (transmitter enable signal) and apply it to the SOA to enable/disable the output of the transmitter. The data modulation is applied to the SL, while the SOA is enabled. As the SOA settling time is 50 ns, the modulating signal to the SL is applied after delay of 50 ns. The optical output is detected using a PIN diode and analyzed using a high-speed sampling oscilloscope. Fig. 10(a) shows the received burst data signal after the PIN photodetector and the corresponding eye pattern (inset). The optical spectrum of the burst mode signal (Fig. 10(b)) is observed using an optical spectrum analyzer set in the maximum hold mode. The OSA resolution is set to 0.02 nm and spectrum is swept until no change in the spectral shape is detected.

Then, post processing is performed to calculate the OOC-PSD at a resolution of 15 GHz. The PSD values are calculated as
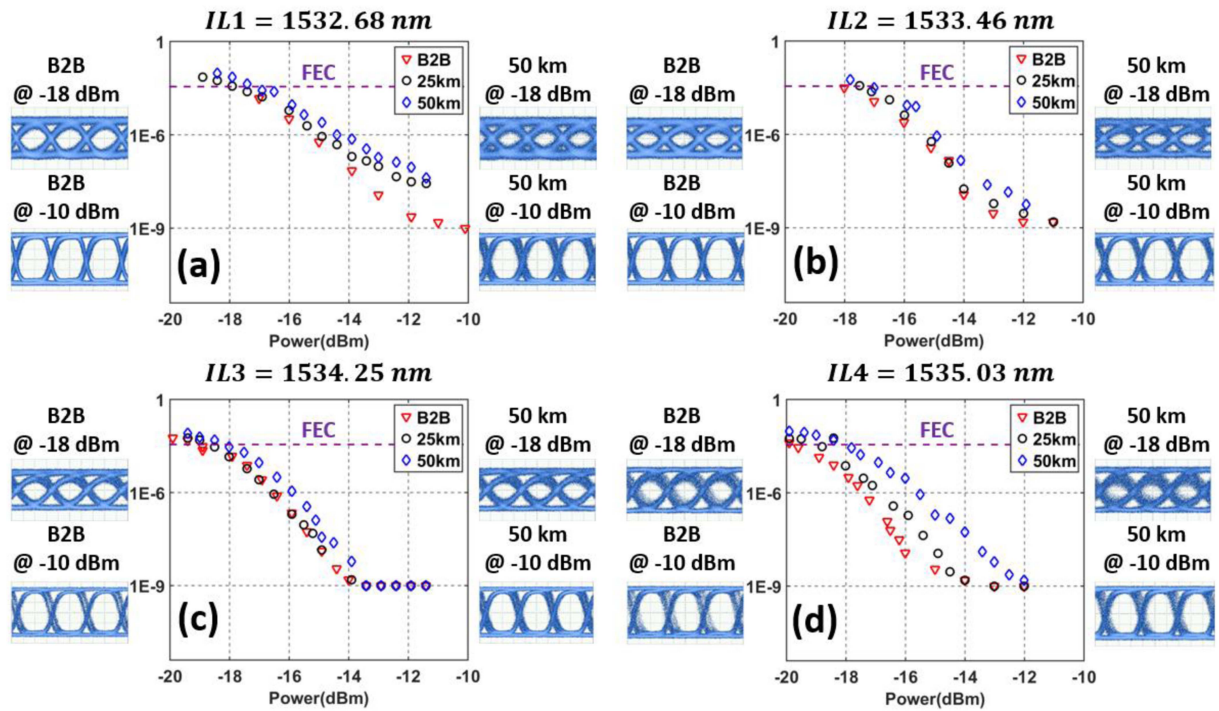
Fig. 8.   (a) BER performance of (a) IL1, (b) IL2, (c) IL3, IL4 (d) Modulated at 10 Gbps. Eyes diagrams in B2B and 50 km transmission case at the corresponding ROP.
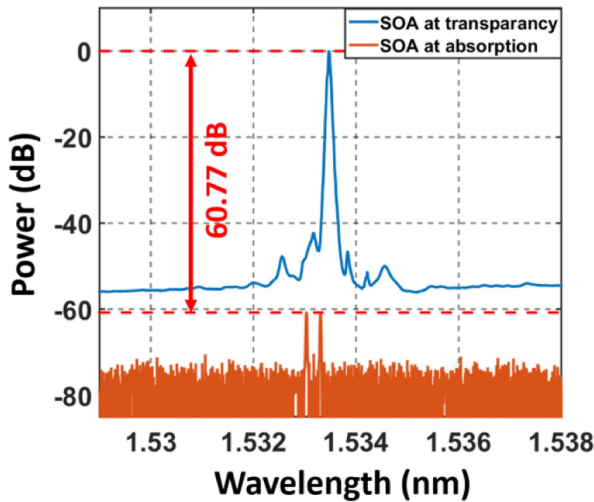

Fig. 9.   Output optical spectrum at forward biased (blue) and reversed biased (orange) SOA.

Fig. 10.   (a) Burst mode data transmission at 62.5 µs burst length at 50% duty cycle and (b) Real-time measurement of spectral excursion.

-44.07 dBm (cyan), -38.29 dBm (green), -41.52 dBm (red), and -46.46 dBm (magenta) at different distances from the operational channel (blue). According to the specification, the maximum OOC-PSD must not exceed -40.5 dBm in case of a 100 GHz channel spacing. All the OOC PSDs are within the limit specified in [8] except channel B that is 1.8 dB higher than the specification. The primary cause of higher PSD in channel B is the side mode of SL falling within the spectral slot of the neighbouring channel, the power of which is further increased when the SOA is directly modulated.
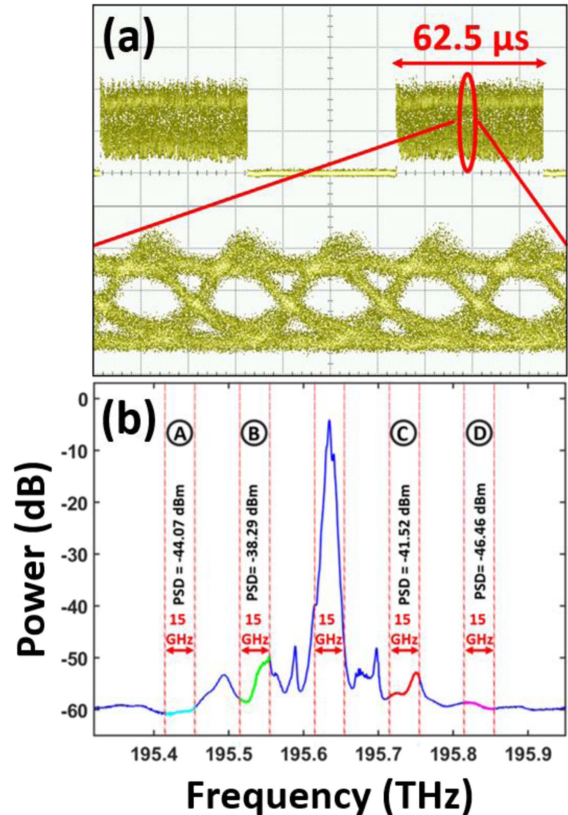
VIII. Conclusion

We have reported on the design, fabrication and detailed characterization of a novel 8-section directly modulated PIC transmitter device suitable for employment in TWDM access networks. A master-slave configuration-based PIC can be tuned to generate four injection-locked, 100 GHz spaced channels. Each of these channels can be modulated at 10 Gbps and the transmission distance can be extended by controlling frequency chirp using an on-chip VOA. We see a significant reduction in the frequency chirp when the ML is turned on and the SL is injection locked. The BER performance at each of the IL wavelengths, when transmitted over 50 km SMF, is well below the forward-error-correction (FEC) limit and always below 5e^{-8}. Furthermore, the integrated SOA at the output of the device enables the optical channel power on-off feature (output optical power below or equal to -62.6 dBm). This PIC also exhibits low level of interference (< -38.29 dBm) to the other equally spaced operational channels. In conclusion, the features of PIC such as ease of fabrication, tunability, error free transmission, low cross channel interference has a potential to be uses as NGPON-2 transmitter with possible improvement in ER and modulation response.

Acknowledgment

References

[1] T. Horvath, P. Munster, V. Oujezsky, and N.-H. Bao, "Passive optical networks progress: A tutorial," *Electronics*, vol. 9, no. 7, Jul. 2020, Art. no. 1081, doi: 10.3390/electronics9071081.

[2] H. S. Abbas and M. A. Gregory, "The next generation of passive optical networks: A review," *J. Netw. Comput. Appl.*, vol. 67, pp. 53–74, May 2016, doi: 10.1016/j.jnca.2016.02.015.

[3] V. Houtsma, A. Mahadevan, N. Kaneda, and D. van Veen, "Transceiver technologies for passive optical networks: Past, present, and future," *J. Opt. Commun. Netw.*, vol. 13, no. 1, pp. A44–A55, Jan. 2021, doi: 10.1364/JOCN.403500.

[4] T. Muciaccia, F. Gargano, and V. Passaro, "Passive optical access networks: State of the art and future evolution," *Photonics*, vol. 1, no. 4, pp. 323–346, 2014.

[5] A. Tavares et al., "Photonic integrated transmitter and receiver for NG-PON2," in *Proc. 2nd Int. Conf. Appl. Opt. Photon.*, vol. 9286, 2014, Art. no. 928605.

[6] K. Fouli and M. Maier, "OCDMA and optical coding: Principles, applications, and challenges [topics in optical communications]," *IEEE Commun. Mag.*, vol. 45, no. 8, pp. 27–34, Aug. 2007, doi: 10.1109/MCOM.2007.4290311.

[7] M. Hu, S. Wu, M. Fang, and L. Tang, "A wavelength reuse OFDM-WDM-PON architecture with downstream OFDM and upstream OOK modulations," in *Proc. IEEE 3rd Int. Conf. Commun. Softw. Netw.*, 2011, pp. 389–392. doi: 10.1109/ICCSN.2011.6013740.

[8] ITU.int.G.989.2, '40-Gigabit-capable passive optical networks 2 (NG-PON2): Physical media dependent (PMD) layer specification,', 2022, Accessed: Jul. 06, 2022. [Online]. Available: https://www.itu.int/rec/TREC-G.989.2-201902-I

[9] E. Kim, S. Moon, M. Sung, H. H. Lee, J. K. Lee, and S. Cho, "Cost-effective photonics-based THz wireless delivery system using a directly modulated DFB-LD," *Opt. Commun.*, vol. 492, Aug. 2021, Art. no. 126969, doi: 10.1016/j.optcom.2021.126969.

[10] N. Andriolli, P. Velha, M. Chiesa, A. Trifiletti, and G. Contestabile, "A directly modulated multiwavelength transmitter monolithically integrated on InP," *IEEE J. Sel. Topics Quantum Electron.*, vol. 24, no. 1, Jan./Feb. 2018, Art. no. 1500306, doi: 10.1109/JSTQE.2017.2746002.

[11] P. Dong, A. Maho, R. Brenot, Y.-K. Chen, and A. Melikyan, "Directly reflectivity modulated laser," *J. Lightw. Technol.*, vol. 36, no. 5, pp. 1255–1261, Mar. 2018, doi: 10.1109/JLT.2018.2791363.

[12] K. Zhong et al., "Experimental demonstration of 500Gbit/s short reach transmission employing PAM4 signal and direct detection with 25Gbps device," in *Proc. Opt. Fiber Commun. Conf.*, 2015, pp. 1–3, doi: 10.1364/OFC.2015.Th3A.3.

[13] D. Li et al., "4×96 Gbit/s PAM8 for short-reach applications employing low-cost DML without pre-equalization," in *Proc. Opt. Fiber Commun. Conf. Exhib.*, 2019, pp. 1–3.

[14] A. Sharma et al., "Wavelength tunable directly modulated laser for TWDM applications," in *Proc. Eur. Conf. Opt. Commun.*, 2021, pp. 1–4.

[15] C. Sun et al., "Modulation characteristics enhancement of monolithically integrated laser diodes under mutual injection locking," *IEEE J. Sel. Topics Quantum Electron.*, vol. 21, no. 6, Nov./Dec. 2015, Art. no. 1802008, doi: 10.1109/JSTQE.2015.2478817.

[16] R. Lang, "Injection locking properties of a semiconductor laser," *IEEE J. Quantum Electron.*, vol. 18, no. 6, pp. 976–983, Jun. 1982.

[17] H. F. Chen, J. M. Liu, and T. B. Simpson, "Response characteristics of direct current modulation on a bandwidth-enhanced semiconductor laser under strong injection locking," *Opt. Commun.*, vol. 173, no. 1–6, pp. 349–355, 2000.

[18] N. Olsson et al., "Chirp-free transmission over 82.5 km of single mode fibers at 2 Gbit/s with injection locked DFB semiconductor lasers," *J. Lightw. Technol.*, vol. 3, no. 1, pp. 63–67, Feb. 1985.

[19] G. Jain et al., "Directly modulated photonic integrated multi-section laser for next generation TWDM access networks," in *Proc. 45th Eur. Conf. Opt. Commun.*, 2019, pp. 1–4.

[20] A. Sharma et al., "A six-section photonic integrated transmitter with chirp control for extension of the transmission reach," *IEEE Photon. J.*, vol. 14, no. 4, Aug. 2022, Art. no. 1540107, doi: 10.1109/JPHOT.2022.3187073.

[21] C. E. Zah et al., "1.5-μm GaInAsP angled-facet flared-waveguide traveling wave laser amplifiers," in *Proc. Opt. Fiber Commun.*, 1990, Paper. THB3, doi: 10.1364/OFC.1990.THB3.

[22] G. Jain et al., "Design optimization for semiconductor lasers with high-order surface gratings having multiple periods," *J. Lightw. Technol.*, vol. 36, no. 22, pp. 5121–5129, Nov. 2018.

[23] A. Roy, S. K. Patra, and T. Piwonski, "Tunable semiconductor slotted lasers for near-infrared optical coherence tomography," *IEEE Photon. Technol. Lett.*, vol. 33, no. 16, pp. 896–899, Aug. 2021, doi: 10.1109/LPT.2021.3098418.

[24] D. Mickus, R. McKenna, and J. F. Donegan, "Large range athermalisation of multi-section surface grating lasers for DWDM-PONs," in *Proc. Conf. Lasers Electro-Opt.*, 2021, pp. 1–2.

[25] M. J. Wallace et al., "Athermal operation of multi-section slotted tunable lasers," *Opt. Exp.*, vol. 25, no. 13, pp. 14414–14426, Jun. 2017, doi: 10.1364/OE.25.014414.

[26] M. Chen, Z. Meng, J. Wang, and W. Chen, "Ultra-narrow linewidth measurement based on Voigt profile fitting," *Opt. Exp.*, vol. 23, no. 5, pp. 6803–6808, Mar. 2015, doi: 10.1364/OE.23.006803.

[27] R. Slavík, J. Kakande, R. Phelan, J. O'Carroll, B. Kelly, and D. J. Richardson, "24 Gbit/s synthesis of BPSK signals via direct modulation of Fabry-Perot lasers under injection locking," in *Proc. 18th Optoelectron. Commun. Conf. Held Jointly Int. Conf. Photon. Switching*, 2013, pp. 1–2.

[28] A. Takada and W. Imajuku, "Linewidth narrowing and optical phase control of mode-locked semiconductor ring laser employing optical injection locking," *IEEE Photon. Technol. Lett.*, vol. 9, no. 10, pp. 1328–1330, Oct. 1997, doi: 10.1109/68.623252.

[29] E. K. Lau, H.-K. Sung, and M. C. Wu, "Frequency response enhancement of optical injection-locked lasers," *IEEE J. Quantum Electron.*, vol. 44, no. 1, pp. 90–99, Jan. 2008, doi: 10.1109/JQE.2007.910450.

[30] E. K. Lau, L. J. Wong, and M. C. Wu, "Enhanced modulation characteristics of optical injection-locked lasers: A tutorial," *IEEE J. Sel. Topics Quantum Electron.*, vol. 15, no. 3, pp. 618–633, May/Jun. 2009, doi: 10.1109/JSTQE.2009.2014779.

[31] A. Villafranca, J. Lasobras, and I. Garcés, "Precise characterization of the frequency chirp in directly modulated DFB lasers," in *Proc. Spanish Conf. Electron. Devices*, 2007, pp. 173–176.